

Temperature Dependent Dynamic Strain Localization and Failure of Ductile Polymeric Rods under Large Deformation

Longhui Zhang^{1*}, Antonio Pellegrino¹, David Townsend¹, Nik Petrinic¹

¹ Department of Engineering Science, University of Oxford, Oxford, OX1 3PJ, U.K.

Corresponding author: longhui.zhang@eng.ox.ac.uk

Abstract

Ductile polymers have been increasingly applied in engineering applications to enhance the structural reliability under impact loading. Due to the limitation of experiment setup to achieve large tensile deformation and the difficulty to achieve dynamic force equilibrium, the localization and post-necking stages up to fracture in the ductile polymers have less been investigated. In the present work, the dynamic strain localization of ductile polymeric rods under large tensile deformation up to fracture is studied on the bespoke Hopkinson tension bar synchronized with a high-speed camera. Transparent polycarbonate (PC) is used as a model material in the present study. Likewise, the constitutive response and fracture behaviour of polycarbonate are also characterized with the assistance of Digital Image Correction (DIC) from low to high strain rates under various temperature conditions. The results quantitatively show that the dynamic local strain rate initially increases dramatically to 200 % of the nominal strain rate due to strain localization. This is followed by a rapid drop with necking propagation, and finally tends to stay at strain rate of approximately 20 % of the nominal strain rate until fracture. The elevated temperatures would result in higher local strain rates. Two constitutive models with and without the consideration of constant strain rate condition are constructed for PC and incorporated in finite element simulations. The trend of dynamic local strain rate history with respect to nominal strain rate is successfully reproduced in simulations. The constitutive models particularly the simple dynamic amplification model, are able to reflect the phenomenological key features of the experimentally observed macroscopic and local responses of polycarbonate, and would find their way into impact resistant transparency applications.

Keywords: Ductile polymer, Strain Localization, Hopkinson bar, Fracture, Local Strain Rate, Numerical Simulation

1 Introduction

Ductile polymers tested in tension undergo an instable homogeneous deformation beyond a certain strain level and localize under decreasing load. This is similar to the behaviour of ductile metals during necking localization [1-4]. However, the localized deformation in the polymer finally ceases and is followed by necking propagation along the specimen gauge section [5]. Nowadays ductile polymers are widely used in aerospace engineering applications and armour design, which are unavoidably subjected to high-speed deformation. It's important to understand the high rate constitutive response and the strain localization in the materials.

The common experimental technique for dynamic strength measurement is the Kolsky bar [6, 7], which is also known as split Hopkinson bar [8]. The dynamic tensile behaviour can be characterized by the split Hopkinson tension bar (SHTB), which consists of the input and output bar sandwiching a dog-bone tensile specimen, since the earliest SHTB design made by our colleagues Harding et al. [9] for the studies of metallic alloys. However, the investigation of polymers using the Hopkinson bar technique brings several challenges. Due to the low impedance of polymer, the transmitted signal is usually too weak to be recorded, or just immersed by the electric noisy signals [10]. In addition, the low modulus of polymer makes it difficult to achieve dynamic force equilibrium [11, 12]. Several attempts have been pursued to overcome these difficulties, such as the pulse shaping technique [13-15], the use of hollow bar [16], polymeric bar [17, 18], quartz gauge [10] and semiconductor strain gage [19] to measure the weak transmitted signal.

Polycarbonate (PC), as a representative thermoplastic polymer, is increasingly employed in various aeronautical and structural engineering applications. For instance, laminated glass, consisting of two glass panels joined with a polymeric interlayer [20-23], has been widely used as transparent armour [24, 25], architectural component [26], windshield [27] of high-speed trains, armed helicopter and airplanes. PC with advantages of low density, high ductility and outstanding transparency is a good candidate for use in laminated glass packages. The transparency subjected to blast impact [28] or bird strike [29] undergoes high-speed deformation [30]. Investigation on the impact resistance of PC is required in order to support analysis of such event and thereby reduce the severity of injuries and ensure safety. It should be noted that before a laminated glass fails dynamically, the PC panel at the rear side jointed with the polymeric interlayer is subjected to large tensile deformation [31]. Moreover, the transparencies in service are experiencing various temperature conditions. *Consequently, it is*

essential to investigate the large tensile deformation and the failure behaviour of PC at different strain rates and temperatures.

Compared to the well documented characterization of the compressive response of PC [32-36], there are a few studies on the tensile behaviour at high strain rates due to the difficulties in the experimental techniques. Savra et al. [37] studied the dynamic tensile behaviour of PC by using a split collar type SHTB and a high-speed camera. Cao et al. [19, 38, 39] reported the dynamic tensile tests using semiconductor strain gages to improve the transmitted signal. Interpolation of SHTB results is subjected to the geometry induced and necking induced stress-strain uniformity issues. Therefore, the SHTB technique with high-speed image analysis can provide the real time monitoring of deformation process and improve the measurement accuracy of the dynamic strain. DIC is a popular non-contact full-field displacement measurement technique. Foster et al. [40] investigated the tensile response of polycarbonate at high strain rates, using DIC technique to measure the local deformation. Tzibula et al. [41] reported the dynamic tensile experiments of PC and analysed the stress and strain evolutions in the specimens. *However, the previous studies mainly reported the dynamic tensile response at relatively low strain level, consequently the large deformation behaviour up to fracture has not been fully addressed, due to the limitation of pulse duration of SHTB apparatus.*

Another related issue is necking localization during dynamic tensile deformation. The previous investigations of PC rarely reveal the localization of the gauge section. A noticeable exception is the very recent work of Tzibula et al. [41], who performed dynamic tensile experiments on PC with an emphasis on material response within the dynamic necking evolution for strain up to 0.4. Recently, Mirone et al. [42-44] and Zhang et al. [45, 46] systematically studied the difference of the local strain and strain rate evolution in the necking zone from the nominal strain and nominal strain rate by combining SHTB and high-speed photography technique, and found that the local strain rate can reach 1000% of the nominal strain rate in metals. *To the best of knowledge, the investigation of dynamic necking-induced local strain rate evolution up to failure in ductile polymers is not yet understood.*

From this brief literature review, it can be observed that a dynamic characterization of the larger tensile deformation and the associated necking evolution of PC are required. Recently, Gerlach et al. [47] designed a new SHTB technique to characterized ductile materials from intermediate to high strain rates. In the present work, tensile experiments under quasi-static, medium rate to high strain rate conditions, assisted by DIC technique [48-50] to accurately measure the strain

history, are carried out to investigate the dynamic local strain rate evolution with respect to the nominal strain rate in a ductile polycarbonate. Likewise, the sensitivities of strain rate and temperature on the tensile constitutive response and failure of PC are also studied. The investigation of large deformation, strain localization and failure behaviour of this ductile thermoplastic polymer will be of considerable interest for engineering applications.

2. Experimental Protocol

2.1 Material and specimens

The polycarbonate specimen was machined to dog-bone shape with threads from a 10 mm diameter rod. Specimens in two dimensions with the gauge length to gauge diameter ratio as 4 mm-4 mm and 8 mm-4 mm are used to achieve various strain rates and strains. After being machined, the specimens were sprayed painted with black ink by using an airbrush in order to produce a random speckle pattern. The diagram of the specimen dimensions is shown in Fig.A1 in Appendix A.

2.2 Experimental setup

The quasi-static tensile experiments at room temperature were carried out using a 50 kN screw-driven Zwick machine. An Image Development Systems (IDS) UEye USB 3.0 Camera was used to monitor the deformation of specimen at a frame rate of 25 fps with an image resolution 2456x2054 pixels. Load was applied at a constant speed corresponding to nominal strain rate of 0.01 /s in displacement control mode. Commercial DIC software LaVision Davis was used to measure the engineering strain of specimen on the mid-section line of gauge section. The medium rate experiments at nominal strain rates from 7-150 /s were carried out using a hydraulic Instron machine 8854, and the specimen deformation process was recorded by a Photron camera with 740x936 pixels image resolution at a frame rate of 10,000 fps.

The high rate experimental apparatus employed in the present work is a bespoke in-house designed 10 mm diameter Hopkinson tension bar [14, 47] (Fig.1). The 2.7 m length incident bar was made of Ti6Al4V alloy, while the 2.7 m length transmitted bar was made of low impedance phosphor bronze. High strain rate tensile tests at elevated temperatures 75 °C and 110 °C were conducted by using an environmental chamber. The mounted specimens were held for 15 minutes before each test to allow the desired temperature to be obtained. A high-

speed Kirana camera was used to monitor the high rate tensile experiments at a framing rate of 1×10^5 fps and exposure time of 2 μ s, providing images with 924x748 pixels resolution.

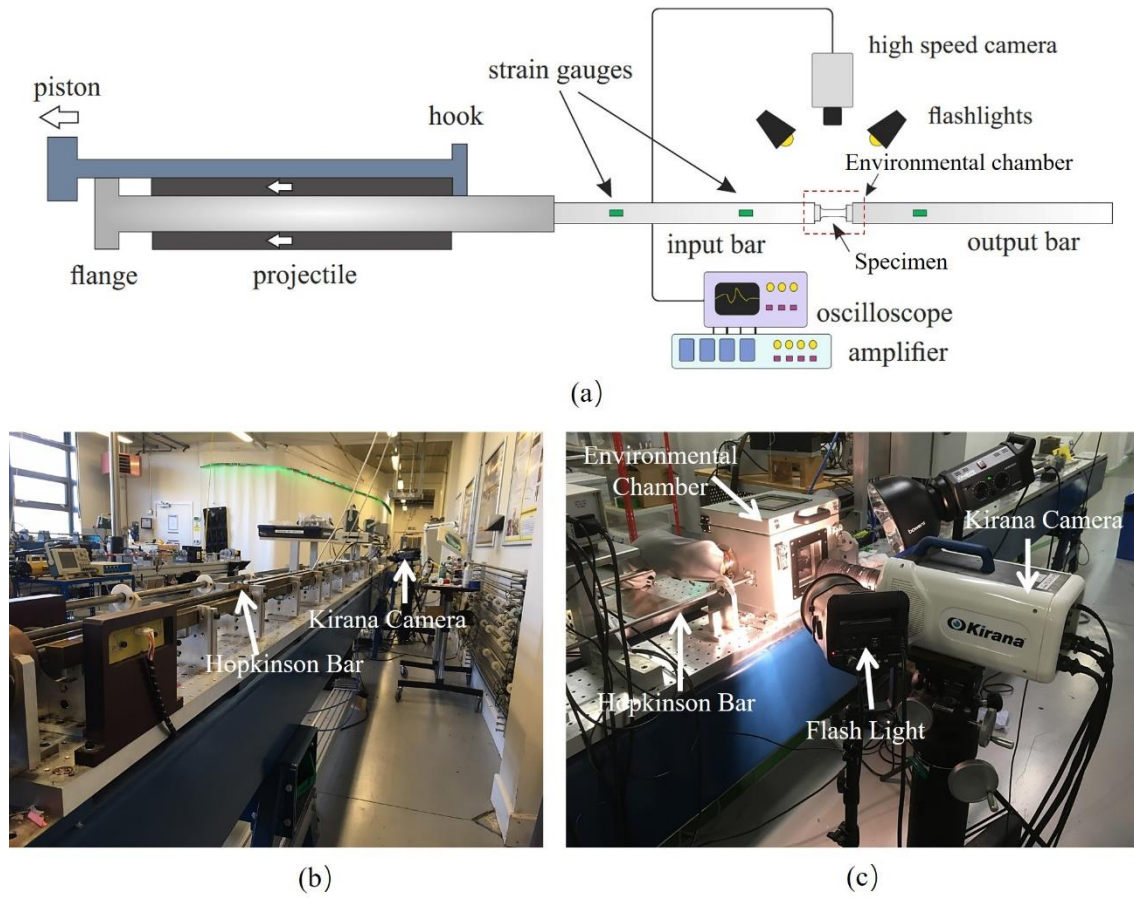


Fig.1. Experimental Setup (a) Schematic of the experimental setup (b) Image of SHTB System (b) Image of Kirana and the environmental chamber setups for elevated temperature tests

In the Hopkinson bar test, when using the 2.5 m long striker made of Ti6Al4V alloy, the stress waves superimpose in the 2.7 m incident bar. An in-house developed algorithm is used to determine the boundary velocities and forces of the specimen by separating the incident and reflected waves in the incident bar. The strain and stress histories are calculated based on the classical Hopkinson bar analysis [51]. The amplitude of propagating wave histories is obtained by the D’Alambert’s solution of wave equations, which was introduced in detail in Ref. [52]. Two strain gauge bridges are attached on the incident bar and one strain gauge bridge is attached on the transmitted bar, and the typical strain gauge signals are shown in Fig.2. The tested specimens and the corresponding conditions are given in Table 1.

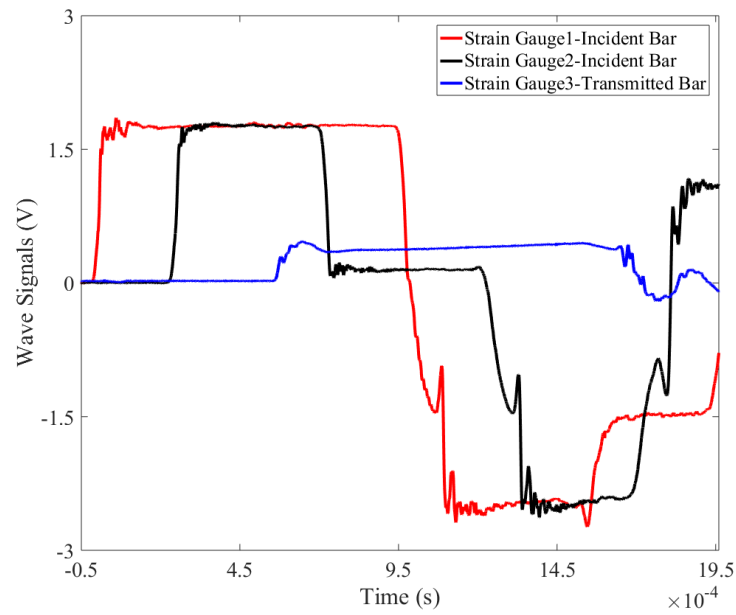


Fig.2 Typical raw signals at nominal strain rate of 1000 /s on the Hopkinson bar. Strain gauge 1 and 2 are attached on the incident bar, while strain gauge 3 is attached on the transmitted bar

Table 1 Summary of tested specimens and the environmental condition

Specimens	Strain rate (/s)	Number of Tests	Condition
4-4	0.01	3	25 °C
4-4	7-150	3	25 °C
8-4	9-95	2	25 °C
4-4	1000-2700	6	25 °C
8-4	1000-2000	3	25 °C
4-4	3100-3300	2	75 °C
8-4	2200	1	75 °C
4-4	3000-3500	2	110 °C
8-4	2000	1	110 °C

3. Experimental Results

3.1 Quasi-static and Medium Rate Experimental Results

Fig.3 shows the engineering stress-strain relationship under quasi-static loading condition with a nominal strain rate 0.01 /s. The engineering stress-strain experiences an initial peak stress about 63 MPa, followed by strain softening during necking, and the cold drawing process with apparent strain hardening. The average engineering strain to failure is approximately 1.30.

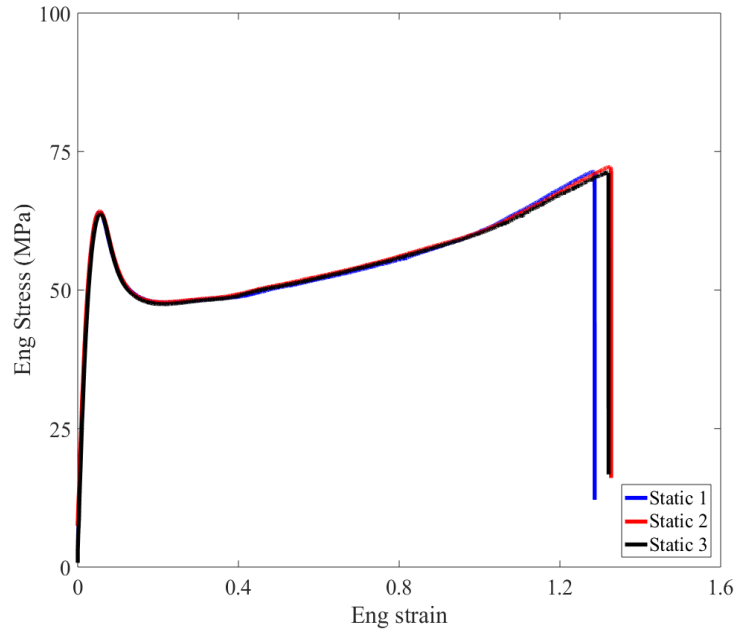


Fig.3 Quasi-static tensile engineering stress-strain relationship of polycarbonate. An initial peak stress can be seen, followed by strain softening and strain hardening.

Fig.4 presents the engineering stress-strain relationship of polycarbonate at medium rates of 7-150 /s. The engineering stress-strain relation from the specimen with 4 mm gauge length and 8 mm gauge length shows almost identical response. The polycarbonate exhibits rate dependent behaviour at medium rates, with an increase in flow stress with strain rate. The force sensor was fixed on the bottom crosshead of the Instron machine. The force measurement shows oscillations for higher strain rates of 150 /s, due to the elastic response and the inertia of the measurement system [53-55]. The failure strain values are generally consistent, apart from one test at 95 /s showing lower failure strain. The average failure strain value 1.35 at medium rate region is slightly higher than the failure strain under quasi-static condition.

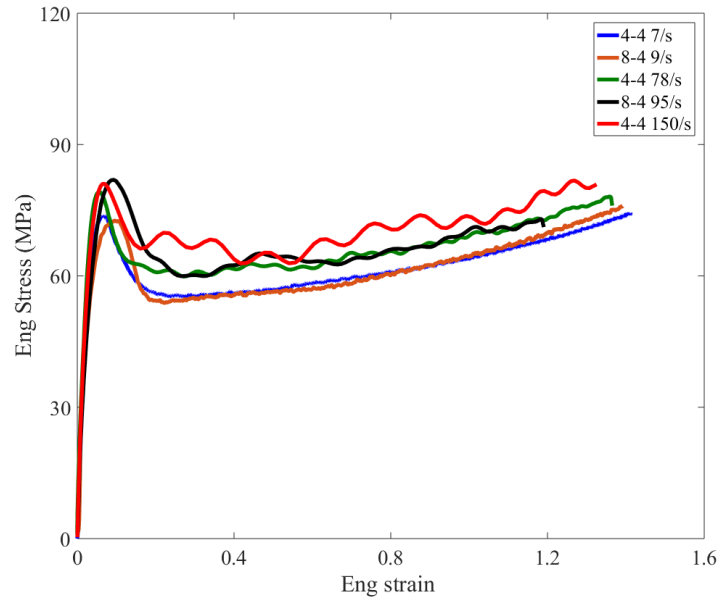


Fig.4 Engineering stress-strain relationship of polycarbonate specimens with the gauge length to gauge diameter ratio as 8-4 and 4-4 at medium rates of 7-150 /s. The polycarbonate shows rate dependent response at medium rates.

3.2 High Rate Experimental Results

High strain rate tests were carried out at nominal strain rates from 900-3000 /s. Dynamic force equilibrium at two ends of the specimen is crucial for valid measurements using Hopkinson tension bar. Fig.5 shows the comparison between the input force obtained from the incident and reflected signals in the incident bar, and the output force measured directly from the transmitted signal in the transmitted bar. By using the present bespoke designed SHTB technique with low impedance phosphor bronze output bar and relatively big specimen with 4 mm gauge diameter and 8 mm gauge length, dynamic force equilibrium can be achieved once the plastic region is entered during the tensile deformation, as reported by Hopperstad et al.[56]. The output force is used for the stress measurement of the specimen.

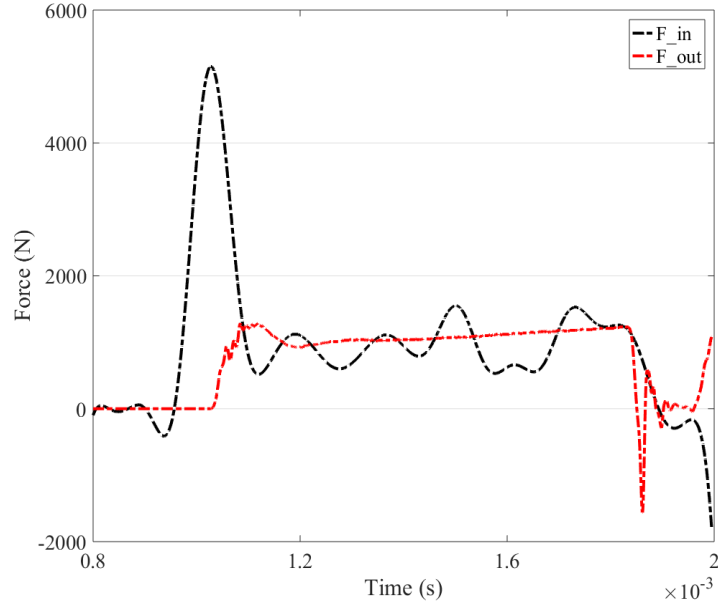


Fig.5 Representative dynamic equilibrium conditions at nominal strain rate of 1900 /s, particularly when the specimen enters plastic deformation zone up to fracture. The output force is measured directly from the transmitted signal in the transmitted bar, while the input force is calculated from the incident and reflected signals in the incident bar.

Fig.6 presents the engineering stress and engineering strain history for 8 mm length specimen at a nominal strain rate of 1900 /s, and the corresponding deformation process is shown in Fig.7 with the image resolution of 41 pixels/mm recorded by the high-speed camera. The engineering stress is calculated based on the transmitted signal from the Hopkinson tension bar, and the engineering strain is directly measured from DIC analysis. The stress increases to 100 MPa at the initial peak and then decreases to 75 MPa due to the necking localization. Later the stress increases to 90 MPa at load drop, at which the engineering strain starts to soar up. From the deformation images in Fig.7, one can observe the necking stage at 177 us, beyond which the localization propagates to the whole gage section and the uniform deformation continues to 677 us. Regarding the failure process, a small crack is noticeable in the gauge section close to the output side (right side) of the specimen. The crack propagates to the whole current cross-section, resulting in the final fracture of the gage section. In addition to the two main separation parts, the fracture cross-section splits into several fragments. Fig.7 also shows that no localized shear band occurs throughout the dynamic large tensile deformation of the polycarbonate rod, which is different from the localization in polycarbonate under plane strain conditions [57].

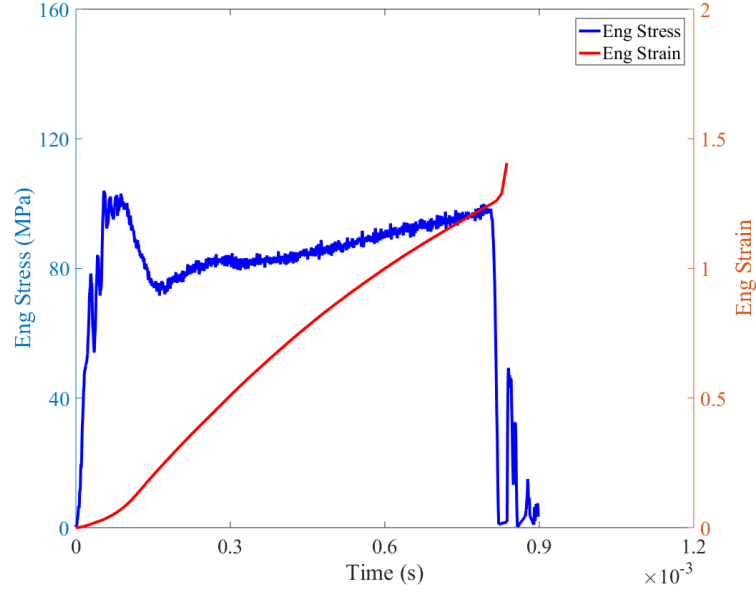


Fig.6 Engineering stress and strain evolutions at a nominal strain rate of 1900 /s. The engineering stress is measured directly from the transmitted signal, while the engineering strain is obtained from DIC analysis.

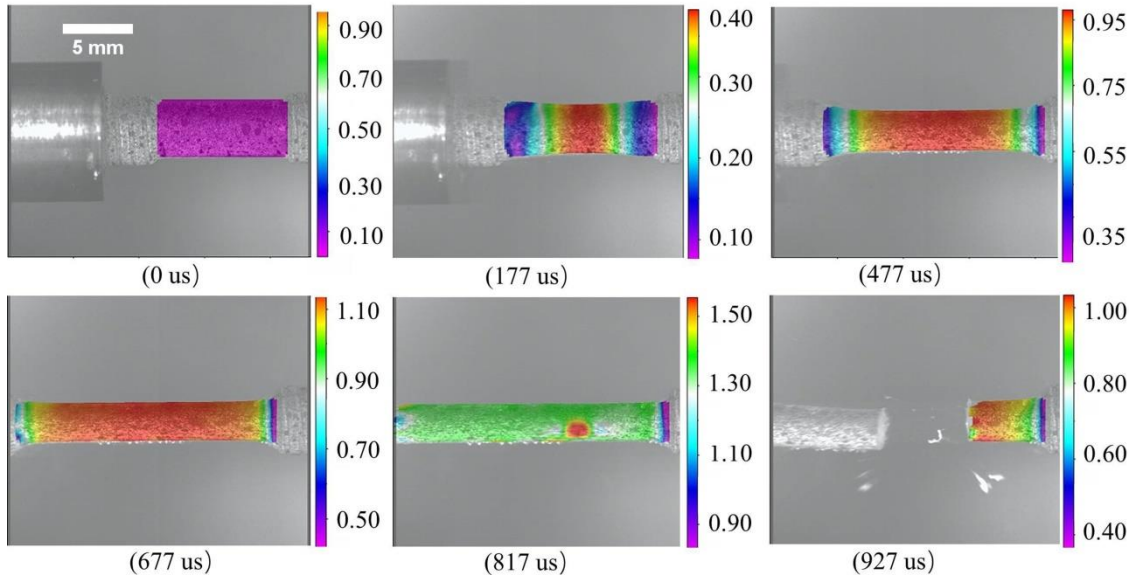


Fig.7 Dynamic deformation process with DIC at nominal strain rate of 1900 /s (*Engineering* axial strain is shown). Five stages with necking localization at 177 us, necking propagation at 477 us, uniform deformation at 677 us, failure at 817 us and fracture at 927 us can be seen.

Fig.8 presents the strain evolution during dynamic tension deformation process. Here, three strain values are compared, namely, the local true strain which is based on the diameter change of minimum cross-section, the macro engineering strain based on the DIC measurement of gauge section elongation, and the widely used macro true strain [19, 37, 41] which is the

logarithmic macro engineering strain. The local true strain ϵ_{LTrue} , macro engineering strain ϵ_{Eng} and macro true strain ϵ_{MTrue} are defined as:

$$\epsilon_{LTrue} = 2 \cdot \log\left(\frac{r_0}{r}\right) \quad (1)$$

$$\epsilon_{Eng} = \frac{L - L_0}{L_0} \quad (2)$$

$$\epsilon_{MTrue} = \log(1 + \epsilon_{Eng}) \quad (3)$$

where r and r_0 are the current and the original radius of the minimum cross section of the specimen, L and L_0 are the current gauge length and the original gauge length. Three regions can be seen in Fig.8. In region 1 the three strain measurements are identical during the uniform deformation process. In strain localization region 2, the macro engineering strain increases gradually. The local true strain, however, presents a sharp increase followed by a modest increase at 300 μ s. The macro true strain increase is slower compared to the above two strain results. In stage 3, the local true strain and the macro true strain are in agreement with from the time 600 μ s to the end of the test. The macro engineering strain shows the highest strain up to specimen fracture. Similar three stages at quasi-static and medium rates can be seen in Fig.A2 in Appendix A.

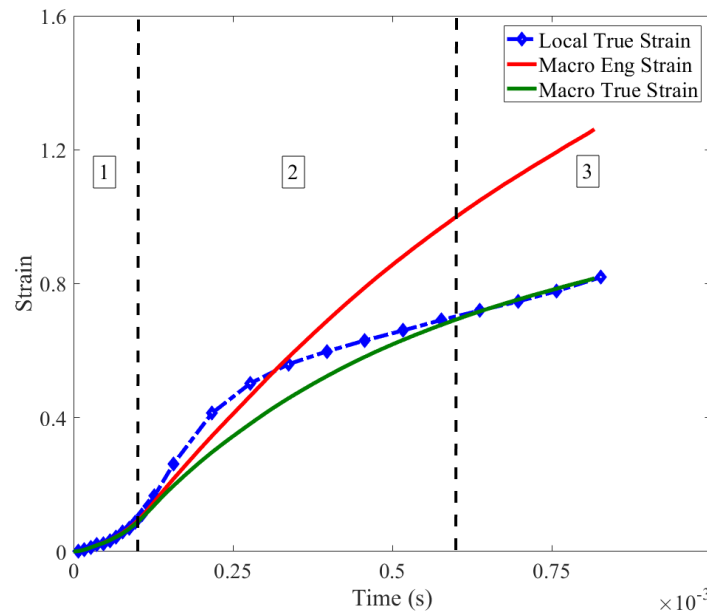


Fig.8 Strain measurements as a function of time during dynamic tensile deformation process at nominal strain rate of 1900 /s. The local strain is directly measured from the diameter change

of the minimum cross-section of neck region, the macro engineering strain is based on the elongation of gauge section, and the macro true strain is logarithmic macro engineering strain

Considering the stress measurement, the local true stress can be calculated as follows:

$$\sigma_{LTrue} = \frac{F}{\pi \cdot r^2} \quad (4)$$

F is the instantaneous force applying on the specimen. Another widely used approach [19, 37, 41] to obtain the true stress of polymers is given by

$$\sigma_{MTrue} = \sigma_{Eng}(1 + \epsilon_{Eng}) \quad (5)$$

where σ_{Eng} is the engineering stress. Fig.9 compares the local true stress and macro engineering stress and the corresponding macro true stress. All stress values decrease after the initial peak stress, due to the strain localization. However, the macro engineering stress in the necking propagation stage only shows a moderate increase, while the local true stress and the macro true stress increase noticeably. One can find that the local true stress is at most 8.3 % higher than the macro true stress in the strain softening region, while they are almost identical in the later uniform deformation stage. The widely used macro true stress is able to represent the local true response with average absolute relative error (AARE) 3.5 %, and consequently could be used to obtain a good estimation of the true stress without undertaking the labour in the diameter measurement of the minimum cross-section in the neck region.

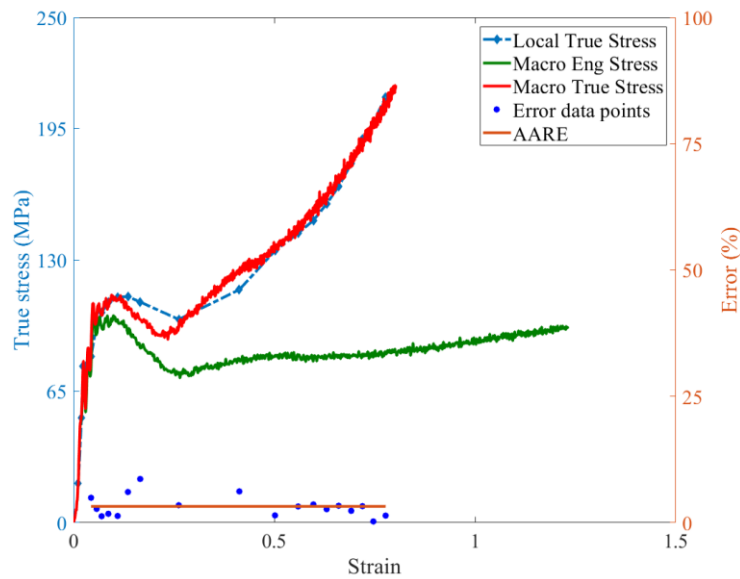
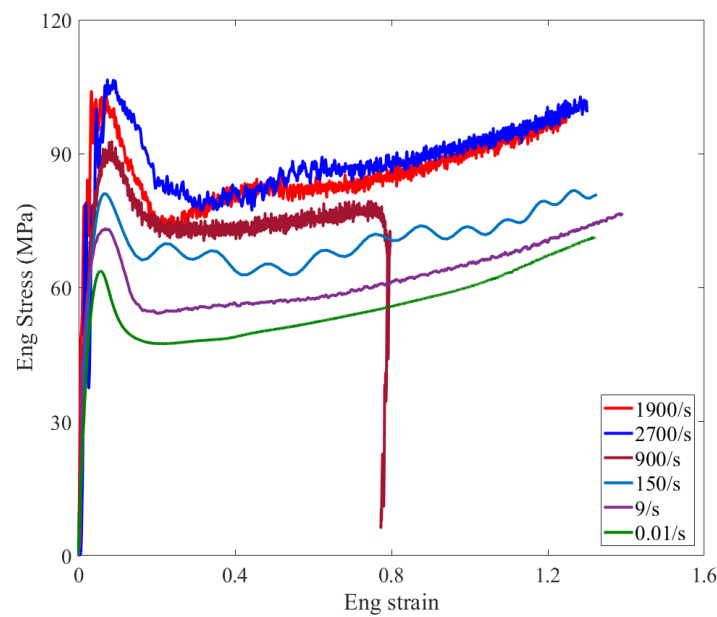
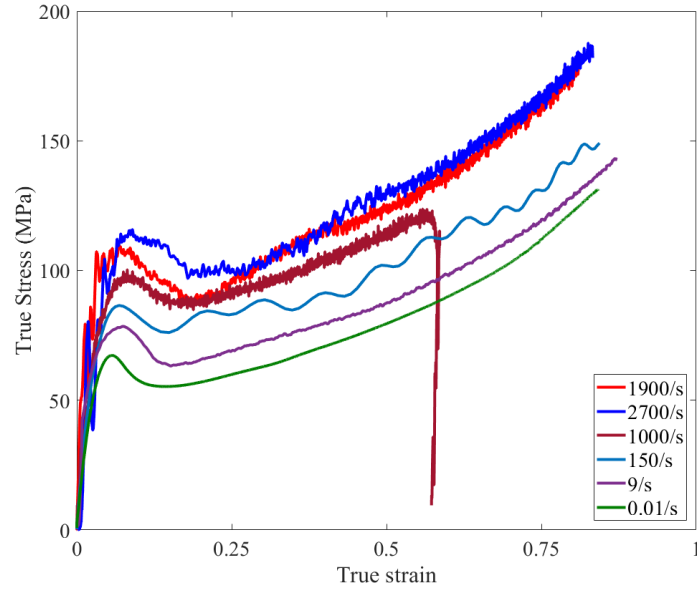


Fig.9 Comparison of different stress-strain relationships and the variation between the macro and local true stress-strain relationship at nominal strain rate of 1900 /s. The red curve is the macro true stress calculated from the macro engineering stress shown in the green curve. Blue dashed line shows the local true stress based on the diameter measurement of necking centre. The error data and average absolute relative error between the macro true stress and local true stress are compared and presented.

Fig.10 summarises the responses of PC under quasi-static, medium to high strain rate loading conditions. The initial engineering peak stress increases from 63 MPa under quasi-static loading to 73 MPa at nominal strain rate of 9 /s and 105 MPa at nominal strain rate of 2700 /s. The strains to failure are not apparently strain rate dependent, compared to the flow stress which presents significant strain rate dependency.



(a)



(b)

Fig. 10 Comparison of (a) engineering stress-strain relation and (b) true stress-strain relation under quasi-static 0.01 /s, medium rates 9 /s and 150 /s, high strain rates of 1000 /s- 2700 /s at room temperature. Note that the unloading during high rate test at strain rate of 1000/s.

The peak true stresses vs nominal strain rate data of PC specimens is summarized in Fig.11, together with the results from the literature [19, 40, 58]. The increasing trend of peak stress in the present paper is consistent with the previously published results. The increasing trend of peak stress in this work can be seen across the nominal strain rates between 10 /s to 1000 /s. Consequently, the combination of the results in the present paper and from the literature provides a better understanding of the tensile peak stress evolution over wide ranges of strain rates for PC.

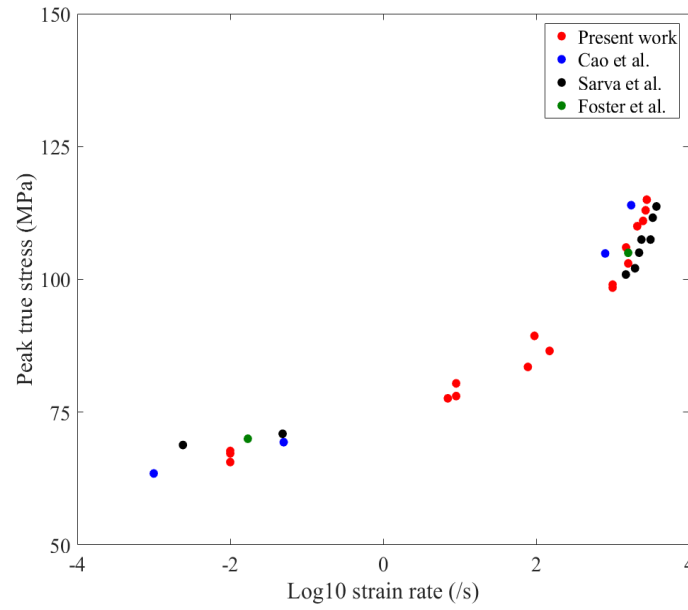
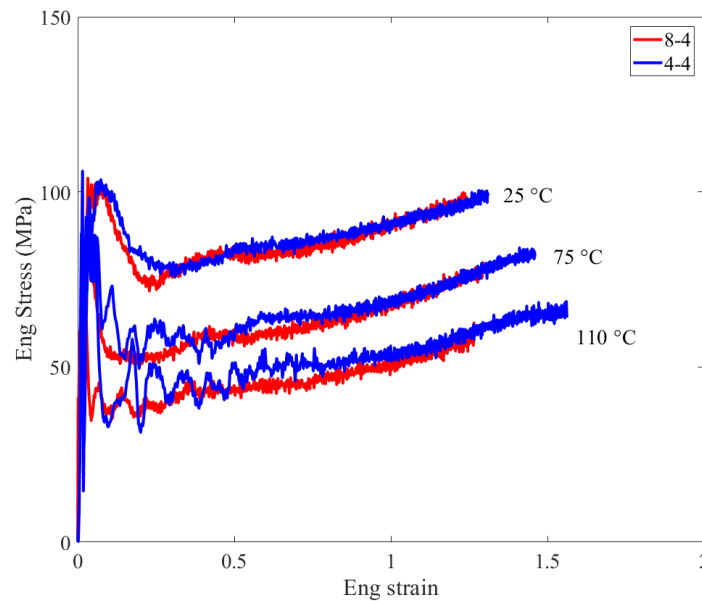


Fig. 11 Comparison of the peak true stress values at various nominal strain rates. The red points are the present results, which cover a wide range of strain rates. Good agreement can be seen between the present measurement and the results from the literature.

Fig.12 shows the engineering and true stress-strain relation at high strain rates at 25 °C, 75 °C and 110 °C. Blue and red curves are the stress-strain relationships obtained from 4 mm and 8mm gauge length specimens, respectively. The flow stress decreases by approximately 20 MPa from room temperature to 75 °C, and declines by approximately 15 MPa from 75 °C to 110 °C. The engineering failure strain at high strain rates increases with temperature, with the average values ranging from 1.3 at 25 °C, 1.4 at 75 °C to 1.6 at 110 °C.



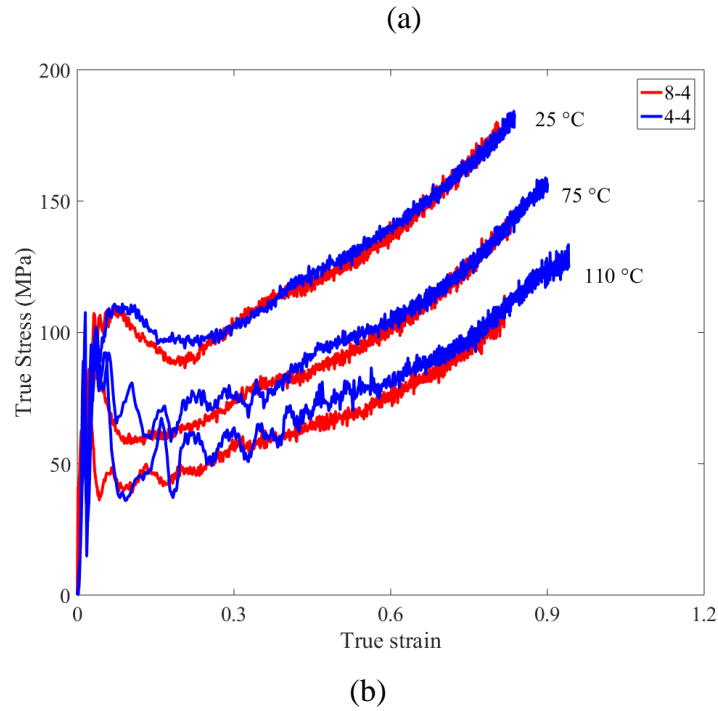
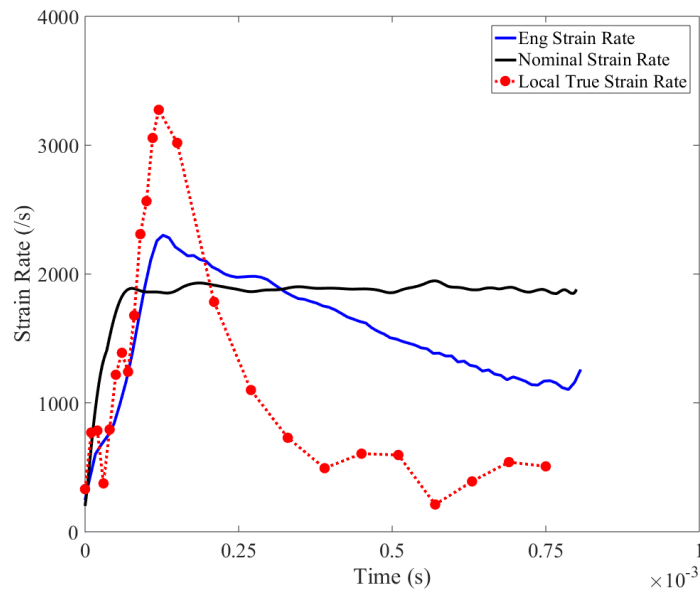


Fig.12 High strain rate (a) engineering stress-strain relationship and (b) true stress-strain relationship at nominal strain rates of 1900-2700 /s at 25 °C, 75 °C and 110 °C. Blue and red curves are for 4 mm and 8mm gauge length specimens, respectively.

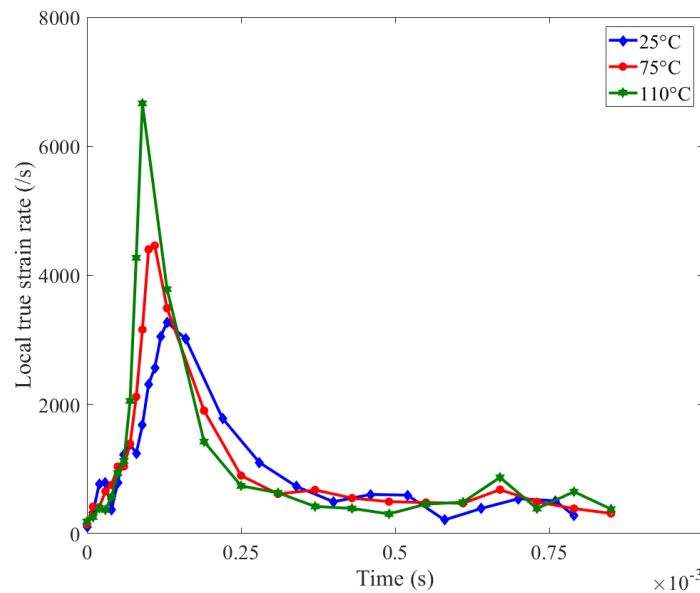
Considering the local strain rate evolution with respect to the nominal strain rate, Fig.13a shows that the peak local true strain rate is higher than the nominal strain rate from Hopkinson bar analysis and the macro engineering strain rate at nominal strain rate of 1900 /s and room temperature. The engineering strain rate is the engineering strain rate of specimen gauge section, while the nominal strain rate is based on the Hopkinson bar analysis of two specimen ends. The local strain rate is determined by the derivative of the local true strain with respect to time as shown in Fig.8. The local true strain rate reaches a peak strain rate of about 3300 /s. Beyond the peak, the local strain rate decreases, when the necking region is propagating in the gauge section. Similar trends can be seen in the engineering strain rate. In contrast, the nominal strain rate from Hopkinson bar analysis is constant at a value of 1900 /s. Beyond the peak, the engineering strain rate is higher than the local true strain rate which is finally constant at strain rate of approximately 500 /s.

Considering the influence of temperature on the local true strain rate, Fig.13b shows the local true strain rate evolutions at room temperature and elevated temperatures at nominal strain rates of 1900-2000 /s. All local strain rate measurements for the three temperatures immediately increase dramatically due to necking localization, followed by a rapid drop and finally a stable

strain rate regime of 400-500 /s. The peak local true strain rate increases with increasing temperature. At high temperatures of 75 °C and 110 °C, the highest local true strain rates are 4800 /s and 7000 /s respectively, compared to the highest local true strain rate at 3800 /s at 25 °C.



(a)



(b)

Fig.13 Strain rate evolution at high strain rates (a) Comparison of strain rate evolution at nominal strain rate of 1900 /s and room temperature. The engineering strain rate of specimen gauge section, local strain rate at the centre of neck and nominal strain rate from SHTB analysis

are compared to show the deviation of strain rate evolution in the specimen (b) Typical local strain rate evolution at nominal strain rates of 1900-2000 /s for room temperature 25 °C and elevated temperatures 75 °C and 110 °C.

As shown in Fig.14, the true stress-strain relation at medium rates under room temperature condition is similar to that at high strain rates at elevated temperature 75°C. The flow stress decreases with temperature while increases with strain rate, indicating the high rate stress–strain relationship at high temperature, agree with the lower strain rate stress–strain relationship at lower temperature.

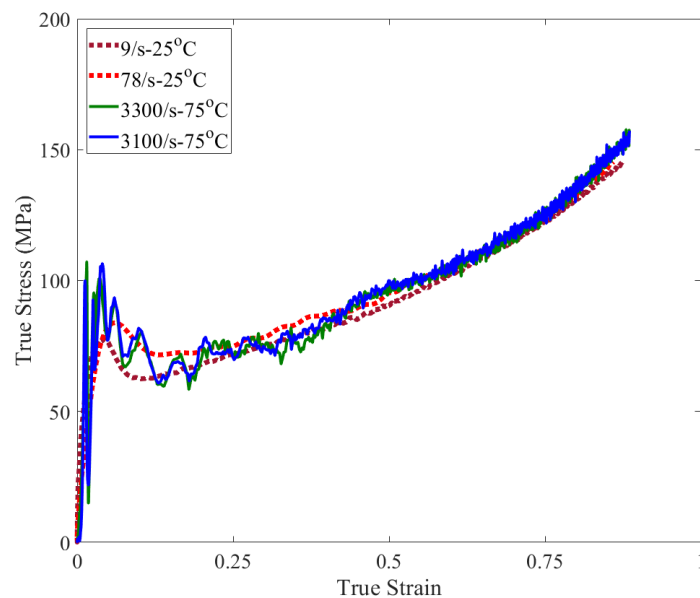


Fig. 14 Comparison between the true stress-strain relation at medium rates and room temperature 25°C, and true stress-strain relation at high strain rates and 75°C. Two dotted lines are the true stress-strain relation at medium rates and room temperature, are compared to the solid lines presenting the true stress-strain relation at high strain rates and elevated temperature 75 °C.

3.3 Microstructural characterization

Fracture surfaces of the tensile polycarbonate specimens were examined using a Carl Zeiss Evo LS15 VP-Scanning Electron Microscope. Fig.15a shows the fracture surface of the specimen failed at nominal strain rate of 0.01 /s at room temperature with hackle lines through the cross-section. Fig.15b shows the specimen which failed at nominal strain rate of 1900 /s at room

temperature. The failure initiates from the top right edge of the specimen and radiates in the craze surface. The failure initiation corresponds to the failure initiation during dynamic deformation process in Fig.7. The fracture morphology in Fig.15c represents the specimen failed at nominal strain rate of 3300 /s and 75 °C, in which a fracture originates from the right edge and spreads along the cross-section, with several ridges characteristics, indicating a slightly increased level of ductility. SEM fractography of the fracture specimen at nominal strain rate of 3000 /s and 110 °C apparently presents a branch of hackle lines along the radiation from the crack nucleation at the bottom edge of the specimen, as can be seen in Fig.15d. Some ridges also form at the edge of the specimen. Similar to the observations in the high-speed image recording, no localized shear band can be seen inside the stretched rods, which is different from the localization under plane strain conditions [57]. The microstructural characterizations reveal the fracture surface of polycarbonate under dynamic tensile loading is characterized by micro brittle fracture manner, in agreement with the findings in Ref. [59].

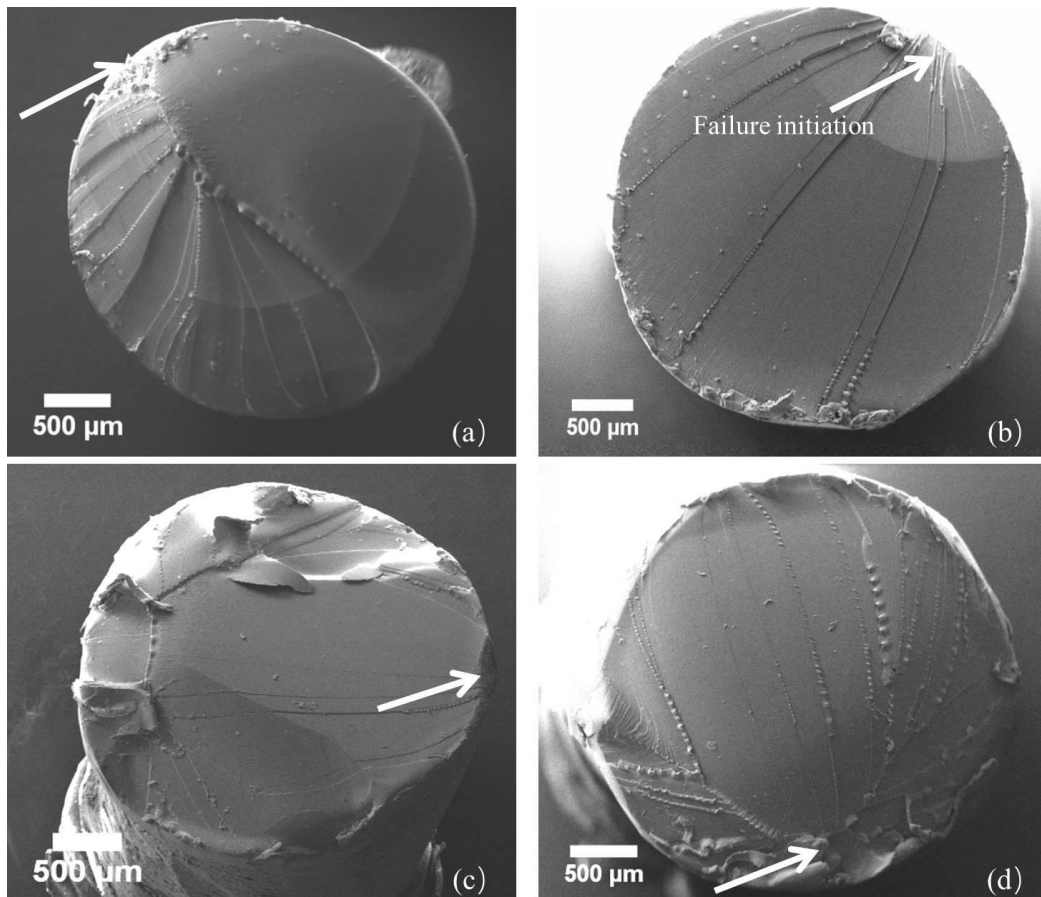


Fig.15 Secondary electron images of fracture surface of specimens tested at (a) quasi-static 0.01/s, 25°C (b) 1900 /s, 25°C (c) 3300 /s, 75°C (d) 3000 /s, 110°C. The failure initiation from the edge of the specimen is arrowed.

4. Constitutive Modelling and Numerical Simulation

4.1 Constitutive Modelling

Finite element simulations are carried out in Section 4 to obtain further insights about the above experimental finding of local strain rate evolution with respect to the nominal strain rate. The selection of the constitutive model of PC for the simulations is important. The tensile responses of PC at various strain rates and temperature show that this material deforms with an initial yield, strain softening and strain hardening. Lu and Ravi-Chandar [60] presented a trilinear stress-strain equation in the quasi-static regime to describe the tensile true stress-strain relationship of polycarbonate. Constitutive models considering the nonlinear relation between the yield stress and the strain rate have been proposed by Richeton et al. [61] and Mulliken and Boyce [32] who also introduced the intrinsic softening behaviour of the material. Cao et al. [19] reported a three-dimensional elastoplastic constitutive model for the tensile deformation of PC. Recently, Tzibula et al. [41] proposed a '4-point model' which can be obtained by multiplying the quasi-static curve by a factor 1.7 to successfully predict the dynamic response of polycarbonate. From the results in the present work, the local true strain rate in the specimen initially increases to twice the nominal strain rate from Hopkinson bar analysis and then decreases to five times lower than the nominal strain rate. This finding, actually, causes difficulties to the constitutive model construction based on a constant rate condition. However, the nominal strain rate from Hopkinson bar analysis, to some extent, could be potentially assumed as an average strain rate of the immediate increase and decrease of local strain rate. Consequently, the nominal strain rate from SHTB analysis is chosen for model calibrations to describe the rate dependent yield behavior, and the strain softening and hardening response of polycarbonate during the necking localization process.

Here, in the spirit of Johnson-cook model [62, 63], an appropriate purely empirical thermal viscoplastic constitutive model (TVM) is proposed to describe the tensile response of polycarbonate, in which the yielding behaviour is described via a Cowper-Symonds model and thermal softening model, and the post-yield regime is described by the conflict and interaction between hardening and softening behaviour. In addition, since there is a strong similarity of the stress-strain relationship under quasi-static, medium to high strain rate conditions, a simple dynamic amplification model (DAM) by multiplying the quasi-static curve by a factor is also adopted to describe the dynamic behaviour of polycarbonate.

4.1.1 Thermal viscoplastic Model (TVM)

The dominant physical behaviour of polycarbonate shows an initial yield at peak stress, followed by the softening softening during necking localization, and the strain hardening due to polymer-chain stretching. The constitutive response of PC can be described by a softening part and a hardening part, with a Cowper-Symonds [64] rate dependent function and a temperature dependent expression as follows:

$$\sigma = A(1 - B\varepsilon_p^n + C\varepsilon_p) \left[1 + \left(\frac{\dot{\varepsilon}}{D} \right)^{1/P} \right] [1 - m(T - T_r)] \quad (6)$$

Where σ is the true stress, ε_p is the plastic strain, A is the peak stress, B and C are softening and hardening parameters. $\dot{\varepsilon}$ is the strain rate, D and P are the parameters describing the strain rate sensitivity, m is thermal softening parameter, T_r is the reference temperature 25 °C.

Dynamic deformation of polycarbonate is associated with thermomechanical coupling induced adiabatic heating effect. Under adiabatic condition, the integration of the stress-thermal balance equation without considering the thermoelastic effect can be given by

$$\beta_{int} \int_0^\alpha \sigma d\varepsilon_p = \rho c_p \Delta T \quad (7)$$

Here, ρ is the density, c_p is the specific heat capacity and ΔT is the adiabatic temperature rise. β_{int} is the Taylor-Quinney factor [65]. Here, the Density 1200 (kg/m³), Specific heat 1300 (J/kg·K) Poisson Ratio 0.33, Young modulus 2 GPa [37, 41, 58, 60], and the Taylor-Quinney factor β_{int} 0.3 [34, 66] are used for the polycarbonate.

At the reference nominal strain rate of 0.01 /s, equation (6) reduces to $\sigma = A(1 - B\varepsilon_p^n + C\varepsilon_p)$. The constants $A = 66$ MPa, $B = 434$, $n = 0.9967$ and $C = 435.65$ can be obtained by the average quasi-static relationship in Fig.3.

Considering the temperature sensitivity, Fig.16 shows results of the average peak stress including standard errors for the PC specimens at high strain rates of 1900-2700 /s for different temperature conditions. The peak stress is found to decrease linearly with temperature increasing from room temperature 25 °C to elevated temperature 110 °C. The temperature dependent parameter m in equation (6) used to describe the thermal (softening) effect, is calculated to be $m = 0.0043$.

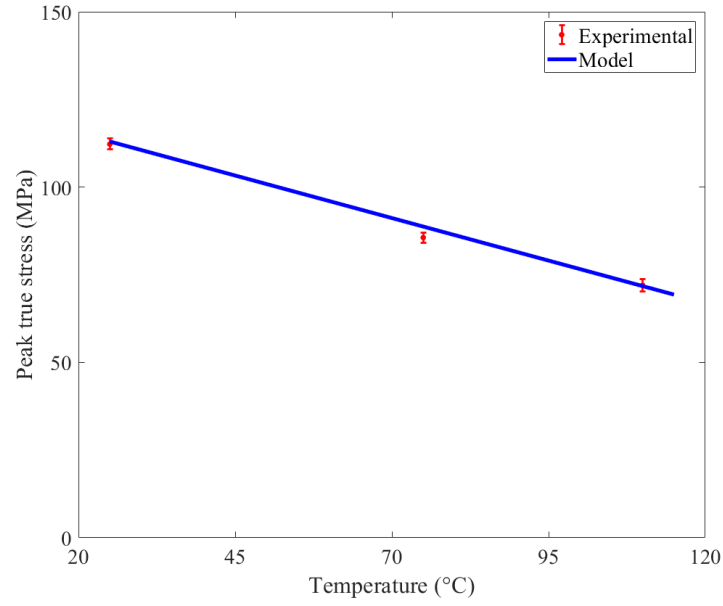


Fig.16 Temperature dependent peak stress of PC specimens at high strain rates. The blue line is the model prediction, compared to the red points showing the average experimental data with the standard error.

Considering the strain rate sensitivity, Fig.17 presents the peak true stress of PC at nominal strain rates from 0.01-3500 /s at room temperature. The peak stress increases nonlinearly with the logarithmic strain rate. Here, a model of Cowper-Symonds rate dependent function in equation (6) is employed to describe the strain rate sensitivity with $D=11928/s$ and $P=4.027$.

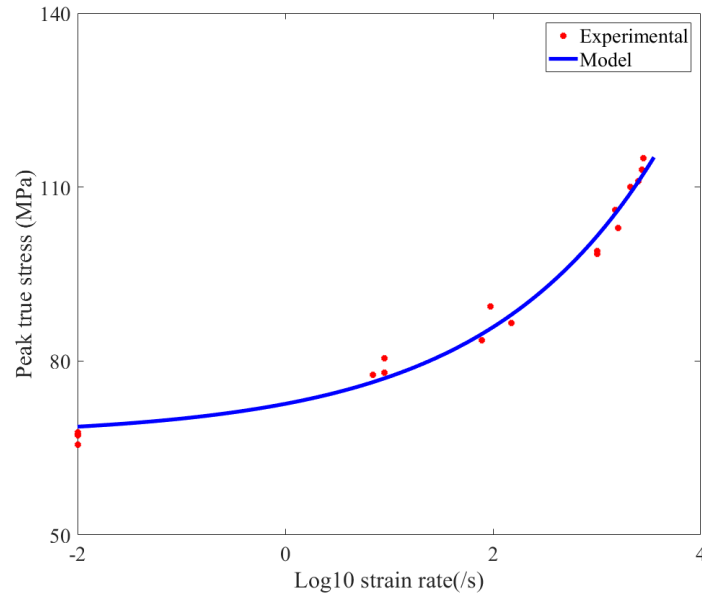


Fig.17 Strain rate dependent peak stress for PC tensile specimens at room temperature. The blue line is the model prediction, compared to the red points showing the experimental peak true stress values

Note that the present softening and hardening, rate dependent and thermal softening model are of the simplest phenomenological nature. More complicated constitutive models developed previously can be found in Refs. [32, 37, 67, 68]. Table 2 summarizes the seven parameters in the constitutive model for polycarbonate material.

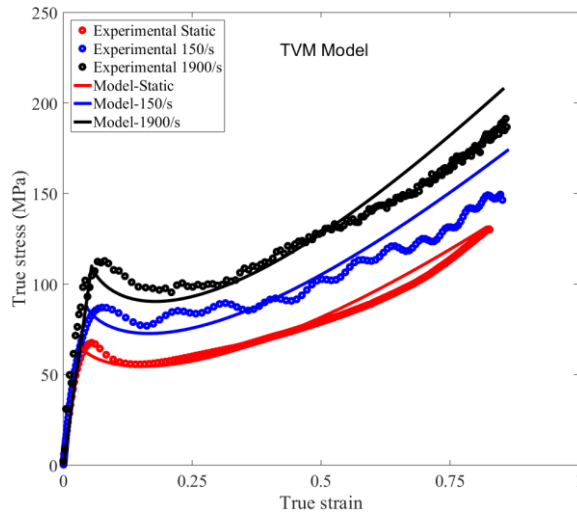
Table 2. Summary of the TVM constitutive relation constants

TVM parameters						
A (MPa)	B	n	C	D (/s)	P	m
66	434	0.9967	435.65	11928	4.027	0.0043

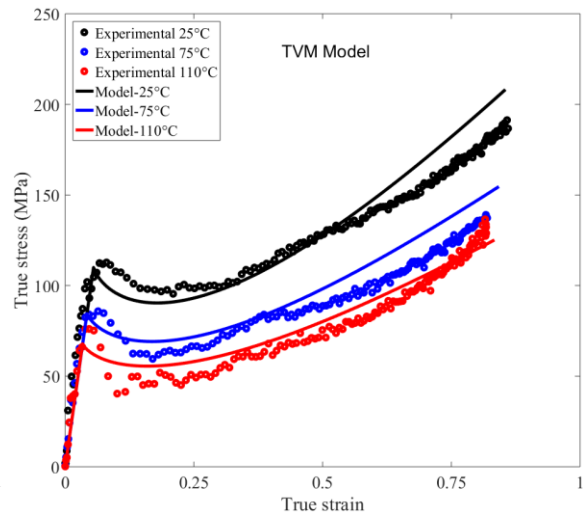
4.1.2 Dynamic Amplification Model (DAM)

A recent analysis [41] indicates that there is a strong correlation between the dynamic and quasi-static behavior of polycarbonate. Due to the similar qualitative and quantitative response in the stress-strain relationship for these two situations, a factor of 1.7 can be used to describe the increase in flow stress from quasi-static to high rate loading. Here, the dynamic model is also

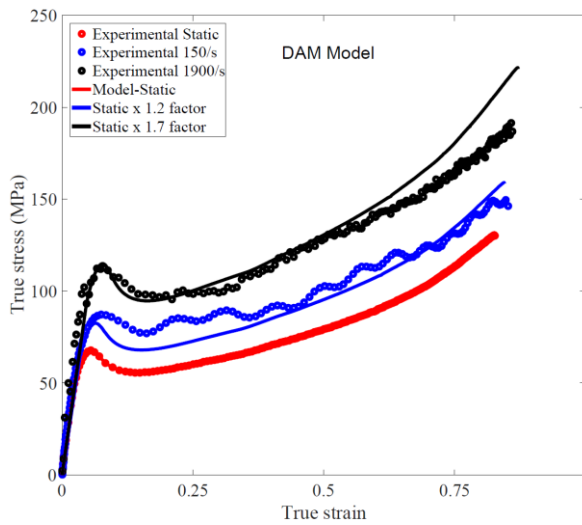
amplified by a factor of 1.7 compared to the static data. Similarly, the model at medium rate is 1.2 greater. Given the equivalent relationship between temperature and strain rate effect for the high strain rate stress-strain data at 75°C and the medium rate stress-strain data at 25°C, the dynamic model at 75°C is also with 1.2 times amplification. Likewise, the dynamic model at 110°C is presented with 0.9 times amplification. Good agreement of the strain rate and temperature dependent response of PC can be seen between the calibrated model data from two models and the experimental true stress–plastic strain relationship in Fig.18. The model predictions show higher stress at true strain beyond 0.6, potentially due to the varying strain rate in the specimen instead of constant nominal strain rate assumed in the model construction.



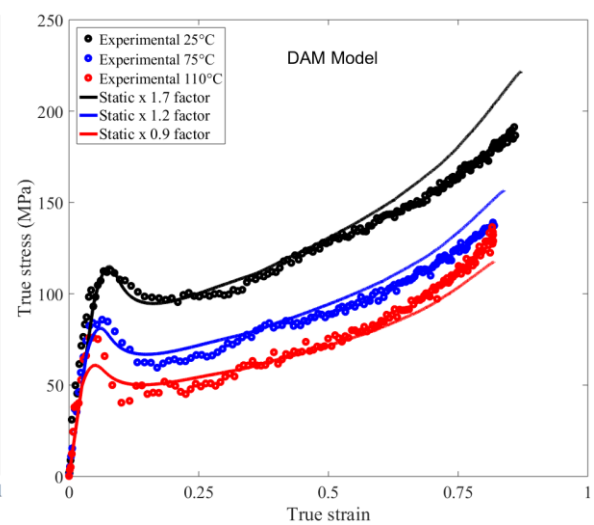
(a)



(b)



(c)



(d)

Fig.18 Comparison between the constitutive relation and the experimental true stress-plastic strain relationship predicted by (a) TVM model at different strain rates and room temperature (b) TVM model at different temperatures and high strain rates (c) DAM model at different strain rates and room temperature (d) DAM model at different temperatures and high strain rates

4.2. Numerical Simulations:

The simulations were performed using ABAQUS [69] in order to demonstrate the key features of the experimentally observed deformation stages using the assumed thermo-viscoplastic model and the dynamic amplification model.

4.2.1 Finite Element Model

In order to decrease the computational time cost, the specimen is modelled as axisymmetric, while the long titanium Hopkinson bar is not included for simplicity. The specimen is meshed with 4-node quadrilateral element (reduced integration element CAX4R) with the size $0.1 \times 0.1 \text{ mm}^2$ for the gauge section and default hourglass control. The mesh convergence was evaluated, in which the differences of critical output force history, stress and strain evolutions and necking position against a measure of mesh density were less than about five percent. The experimentally measured incident and transmitted velocities are used as the boundary conditions at the specimen edges, as can be seen in Fig. 19. The TVM model is implemented into ABAQUS through a VUMAT subroutine [70]. Regarding the simulations by using the DAM model, the true stress-true plastic strain data generated from the dynamic amplification model is a direct input into the ABAQUS as the plastic constitutive description, with the Young modulus 2.0 GPa, Density $1220 \text{ (kg/m}^3\text{)}$, Poisson Ratio 0.40.

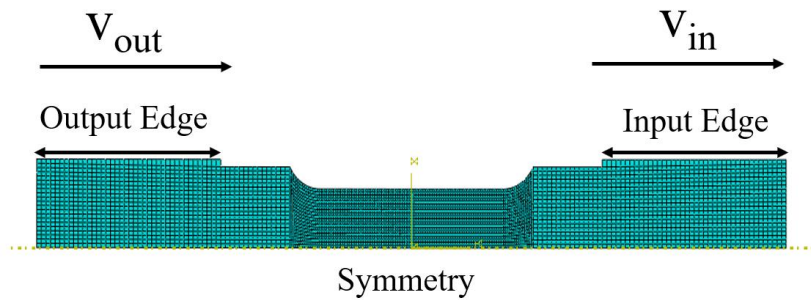


Fig.19 Geometry and boundary conditions of the specimen in simulations. The velocity

boundary conditions are applied at the edges of two specimen shoulders.

4.2.2 Simulation Results:

A typical deformation profile of specimen with 8 mm gauge length at 1900 /s is shown in Fig.20. The deformation corresponds to a displacement of 3.2 mm, and the logarithmic strain contours are given in each profile. The simulations from the two models give similar strain contours. The current minimum diameters 3.16 mm and 3.18 predicted by thermal viscoplastic and dynamic amplification models are consistent with the experimentally measured minimum diameter 3.17 mm.

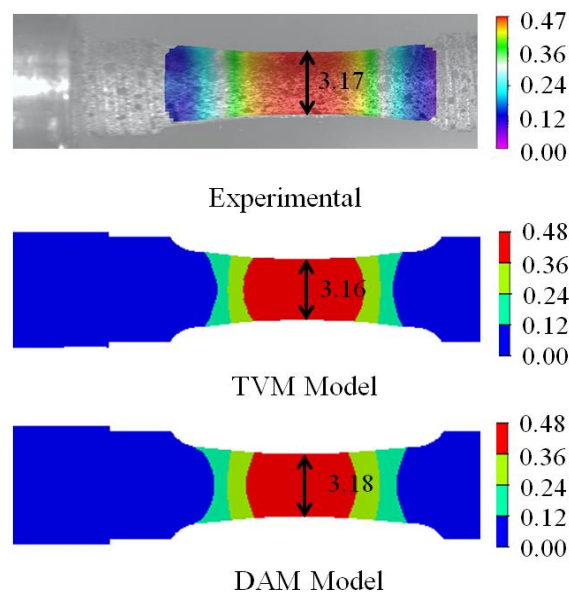
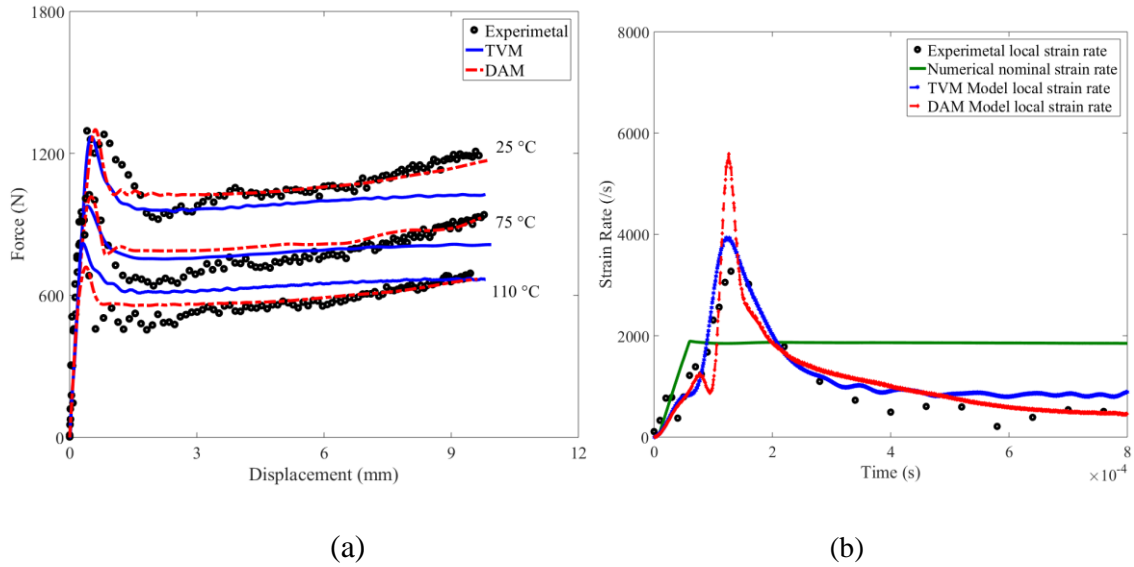


Fig.20 Typical necking profile predicted by two models at nominal strain rate of 1900 /s. The current minimum diameters from the simulations are compared to the experimental measurement.

Fig.21a compares the experimental and numerical tensile force-displacement data of the 8 mm gauge length specimen at 25 °C, 75 °C and 110 °C and nominal strain rates of 1900 /s-2000/s. The force is the reaction force from the specimen, while the displacement is based on the elongation of the specimen gauge length. The numerical global tensile force-displacement relationship is in agreement with the experimental measurements qualitatively and quantitatively. A peak force is observed in the response indicating the following dynamic strain localization.

Compared to TVM model, the numerical force-displacement from DAM model shows higher hardening behavior and consequently agrees more with the experimental results. Fig.21 (b-d) show the simulated strain rate histories at 25 °C, 75 °C and 110 °C and nominal strain rates of 1900 /s-2000/s, in order to reveal the trend of experimental observed local strain rate evolutions. The local strain rate immediately increases to twice nominal strain rate due to strain localization. Then the local strain rate decreases rapidly as the localization propagates throughout the gauge section. Identical trends can be seen in both numerical and experimental local strain rate histories. Beyond 400 us, the local strain rates stay at a low strain rate region about 20% of the nominal strain rate, indicating the local strain rate is not constant during the dynamic tensile deformation of polycarbonate. The local strain rate histories from the simulation and experiment give identical trends of the local strain rate evolution. Note that the local strain rate evolutions from DAM model shows a better agreement with the experimental results, in terms of the dramatic increase and the decrease of the strain rate with respect to the constant nominal strain rate and its temperature dependency.



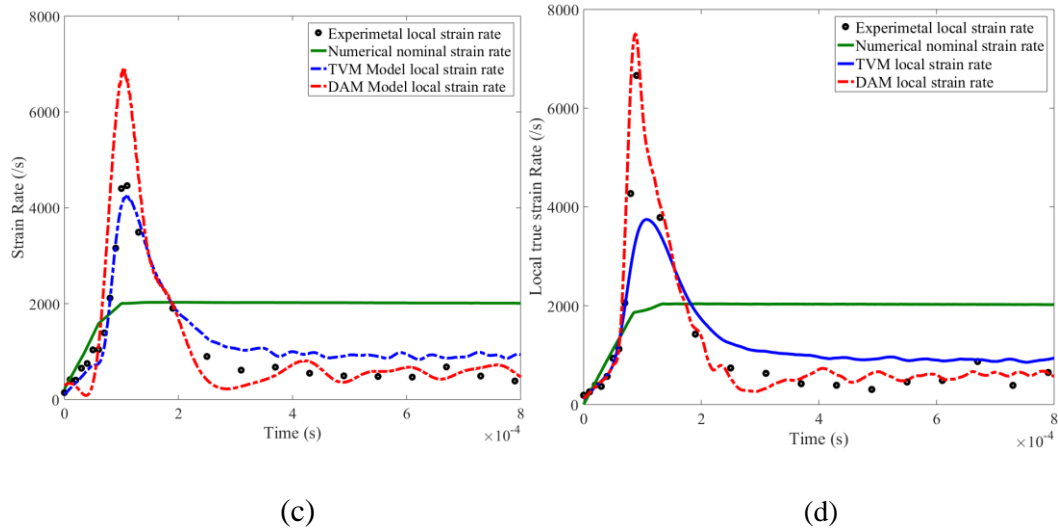


Fig.21 The comparison between the experimental and numerical (a) macro force-displacement, and the strain rate histories between the numerical results and experimental measurements at (b) 25 °C, (c) 75 °C and (d) 110 °C at nominal strain rate of 1900-2000 /s. The experimental force-displacement data in black color is compared to the prediction from two models. The experimental local strain rate histories are compared to the local strain rate evolutions from two model predictions, together with the nominal strain rate.

Fig.22 compares the experimental and numerical dynamic local true stress-strain relationship at room temperature 25 °C, elevated temperatures 75 °C and 110 °C at nominal strain rates of 1900 /s-2000/s for specimens with 8 mm gauge length. The simulated true stress and true strain are the values calculated from the diameter at the centre of the neck using the equations (1) and (4). The predicted local true stress-strain relationships from the two models show both the strain localization softening and strain hardening observed in the experimental measurements at three temperatures. Here, the local behavior from DAM model also presents more strain hardening than that from TVM model, consequently in better agreement with the experimental results.

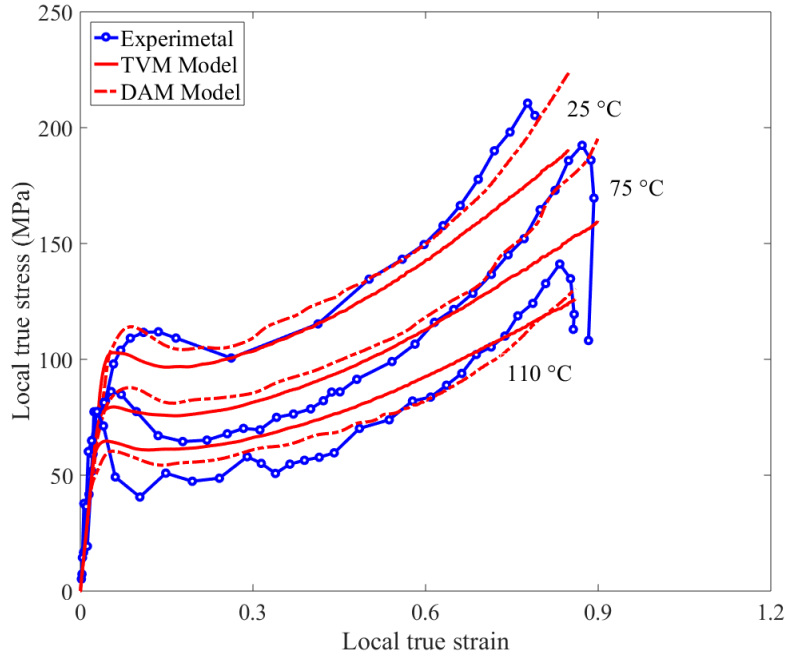


Fig.22 Comparison between the numerical and experimental local true stress-strain relationship at 25 °C, 75 °C and 110 °C at nominal strain rates of 1900-2000/s. The blue line and points show the experimental local true stress-strain relation which are compared to two model predictions at these three temperatures.

5. Discussion

This paper reports the large tensile deformation and failure behaviour of ductile polymeric rods from low to high strain rates at different temperatures, by using polycarbonate as a model material. This material has been increasingly used in the design of a transparency in aerospace engineering to improve the structural impact resistance, e.g. against bird strike events [27, 29]. The present work characterizes the dynamic strain localization in PC, by using a bespoke designed SHTB technique synchronized with a high-speed camera. With the use of a low impedance phosphor bronze output bar with relatively big specimen with 4 mm diameter gauge section, dynamic force equilibrium can be achieved during dynamic deformation. The corresponding image analysis provides an accrue strain measurement under large tensile deformation up to fracture, and the measurement of true stress-strain relationship and local true strain rate evolution of the neck region.

The initial peak stress increases from quasi-static loading condition to medium and high strain rates. The failure strain at room temperature is found to be rate independent, compared to the temperature dependency. The typical dynamic tensile failure process is recorded: A craze crack is evident on the gage surface, followed by the crack propagating to the whole cross-section, which results in the final fracture of specimen. The microstructural characterization shows the fracture surface of polycarbonate under dynamic tensile loading is characterized by micro brittle fracture, in contrast to the significant macro ductility. The lack of micro ductility and the anomalous impact properties are thought to be a result of a chain disentanglement mechanism which is unique to polycarbonate [59].

Regarding dynamic necking localization, Mirone et al. [42-44] and Zhang et al. [45, 46] recently reported the difference of the local strain and strain rate evolution in the necking zone of metals from the nominal strain rate based on the Hopkinson bar principle. Similarly, the results of the necking in polycarbonate specimens also show that the local strain rate is quite different from the nominal strain rate from Hopkinson bar analysis. However, compared to the necking in metals where the local strain rate can reach one order of magnitude higher than the nominal strain rate, the local strain rate in polycarbonate is initially twice the nominal strain rate during strain softening, and then decreasing to one order of magnitude lower during the later uniform deformation process. This information is also important in order to understand the failure of polycarbonate, since the material fails at a very low local strain rate typically of several 100 /s, regardless of the nominal strain rate of several 1000 /s. The nominal strain rate from Hopkinson bar analysis fails to reflect the actual strain rate evolution in the specimen gauge section.

Regarding the constitutive modelling, the local true strain rate differs from nominal strain rate. However, the nominal strain rate can potentially represent an average strain rate of the immediate increase and decrease of local strain rate. In addition, although the local true stress agrees with the macro true stress in the later uniform deformation stage, the local true stress is higher than the macro true stress in the strain softening region. It's found that the macro true stress is able to represent the local true response with average absolute relative error 3.5 % and consequently is suggested to be a good estimation of the true stress of the specimen, as referred in [19, 37, 41].

An appropriate purely empirical TVM model is proposed to describe the tensile response of polycarbonate, in which the plastic deformation is described by the conflict between softening

and hardening behaviour, with Cowper-Symonds rate dependency and linear thermal softening model. Likewise, a DAM model is also proposed based on the similarities of the stress-strain relation at various strain rates, which indicates the strong connection of the stress-strain relation under quasi-static and high strain loading conditions, as suggested by Tzibula et al. [41]. The constitutive relations at high rate and medium rate are presented by multiplying the quasi-static curve by different factors.

The numerical simulations are conducted, in order to evaluate the experimental observed macro response and the dynamic local strain rate history. The numerical force-displacement data from two models particularly the DAM model, agrees with the temperature dependent experimental data, indicating the suitability of the constitutive models in the prediction of the dynamic response of the polycarbonate. Considering the local true stress-strain relationship, the simulated true stress-strain relationship displays the strain localization softening and strain hardening observed in the experimental measurements. Both local strain rate evolutions from the simulation and experiment show identical trend of the local strain rate history with respect to the nominal strain rate. There are some variations between peak strain rate from the simulation and experiment, which is potentially due to the assumptions of constant material properties of polycarbonate at different strain rates and temperatures for simplification, and the choice of constitutive model parameters [71].

Both of the constitutive models are able to capture the basic features of the tensile response. Further work will focus on the dynamic mechanical behaviour of polycarbonate under different triaxiality stress conditions. The DAM model easily extracted from the quasi-static behaviour provides a convenient modelling of dynamic constitutive response of ductile polycarbonate, which should find its way in impact resistant transparency application.

6. Conclusion

This paper presents dynamic strain localization and the constitutive response of a transparent polycarbonate under large tensile deformation. The stress-strain relationship of polycarbonate displays significant strain rate dependency. The dynamic local strain rate jumps during strain softening, then decreases with necking propagation, and eventually becomes constant at strain rate about 5 times lower until fracture occurs. Note that the material fails at a low local strain rate even at high rate loading condition. The constitutive behaviour of PC shows the initial peak stress and the ultimate stress increases from quasi-static to medium and high strain rate

loading conditions. The failure strain values are not apparently strain rate dependent, while the temperature dependent failure strain is obvious. The Cowper-Symonds model is found to be able to describe the rate dependent peak stress under tension loading mode. Two simple TVM and DAM constitutive models are used to describe the dynamic response of polycarbonate. The trend of dynamic local strain rate evolution of specimens is reproduced in numerical simulations. The DAM model can be very easily extracted from the quasi-static behaviour of the material with a better predictions of the experimental results, would be a convenient and beneficial tool for transparency design purposes.

Acknowledgements:

The assistance from Mr. Stuart Carter, Dr. K.Dragnevski and Dr. M.Tkaczykfor and Mrs. Karen Bamford is greatly appreciated

Declaration of interests

The authors declare that they have no known competing financial interests or personal relationships that could have appeared to influence the work reported in this paper.

Appendix A

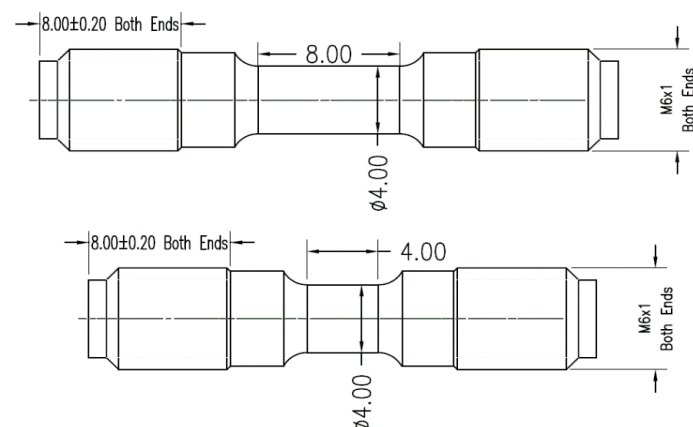


Fig.A1 Geometry of the specimens (all dimensions in mm). 8 mm gauge length and 4 mm gauge length specimen are used to achieve various strain rates

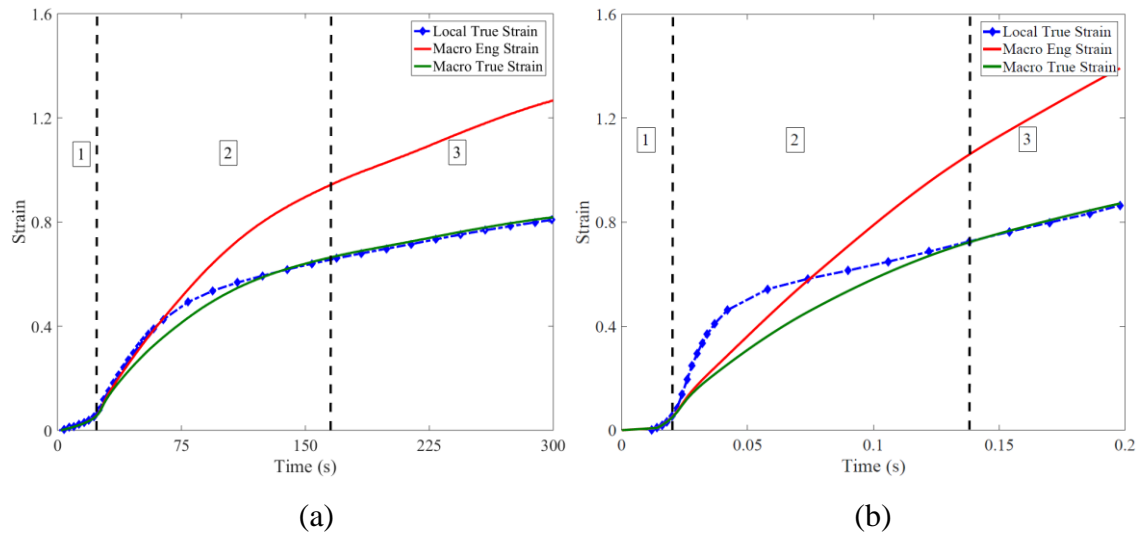


Fig.A2 Strain measurements as a function of time during dynamic tensile deformation process at (a) quasi-static and (b) medium rate of 9 /s. Three stages can be seen during the deformation, which are similar to those at high strain rates.

References

- [1] A. Needleman, A numerical study of necking in circular cylindrical bar, *J Mech Phys Solids*, 20 (1972) 111-127.
- [2] V. Tvergaard, A. Needleman, Analysis of the cup-cone fracture in a round tensile bar, *Acta Metallurgica*, 32 (1984) 157-169.
- [3] A. Vaz-Romero, Y. Rotbaum, J. Rodríguez-Martínez, D. Rittel, Necking evolution in dynamically stretched bars: New experimental and computational insights, *J Mech Phys Solids*, 91 (2016) 216-239.
- [4] D. Macdougall, J. Harding, The measurement of specimen surface temperature in high-speed tension and torsion tests, *Int. J. Impact Eng*, 21 (1998) 473-488.
- [5] K. Neale, P. Tuğcu, Analysis of necking and neck propagation in polymeric materials, *J Mech Phys Solids*, 33 (1985) 323-337.
- [6] H. Kolsky, An investigation of the mechanical properties of materials at very high rates of loading, *Proceedings of the Physical Society. Section B*, 62 (1949) 676.
- [7] H. Kolsky, *Stress waves in solids*, Courier Dover Publications, 1963.
- [8] B. Hopkinson, A method of measuring the pressure produced in the detonation of high explosives or by the impact of bullets, *Proceedings of the Royal Society of London. Series A*, 89 (1914) 411-413.

- [9] J. Harding, E. Wood, J. Campbell, Tensile testing of materials at impact rates of strain, *J. Mech. Eng. Sci*, 2 (1960) 88-96.
- [10] W. Chen, F. Lu, B. Zhou, A quartz-crystal-embedded split Hopkinson pressure bar for soft materials, *Exp Mech*, 40 (2000) 1-6.
- [11] B. Song, W. Chen, Dynamic stress equilibration in split Hopkinson pressure bar tests on soft materials, *Exp Mech*, 44 (2004) 300-312.
- [12] B. Briscoe, R. Nosker, The influence of interfacial friction on the deformation of high density polyethylene in a split Hopkinson pressure bar, *Wear*, 95 (1984) 241-262.
- [13] W.W. Chen, B. Song, Split Hopkinson (Kolsky) bar: design, testing and applications, Springer Science & Business Media, 2010.
- [14] R. Gerlach, S.K. Sathianathan, C. Siviour, N. Petrinic, A novel method for pulse shaping of Split Hopkinson tensile bar signals, *Int. J. Impact Eng*, 38 (2011) 976-980.
- [15] X. Nie, B. Song, Y. Ge, W. Chen, T. Weerasooriya, Dynamic tensile testing of soft materials, *Exp Mech*, 49 (2009) 451-458.
- [16] W. Chen, B. Zhang, M. Forrestal, A split Hopkinson bar technique for low-impedance materials, *Exp Mech*, 39 (1999) 81-85.
- [17] M.Y. Leung, T. Yu, Dynamic characterization of micro-scaled samples using the Hopkinson tensile bar technique, *The Journal of Strain Analysis for Engineering Design*, 43 (2008) 595-607.
- [18] T. Johnson, S. Sarva, S. Socrate, Comparison of low impedance split-Hopkinson pressure bar techniques in the characterization of polyurea, *Exp Mech*, 50 (2010) 931-940.
- [19] K. Cao, Y. Wang, Y. Wang, Experimental investigation and modeling of the tension behavior of polycarbonate with temperature effects from low to high strain rates, *Int J Solids Struct*, 51 (2014) 2539-2548.
- [20] L. Zhang, X. Yao, S. Zang, Q. Han, Temperature and strain rate dependent tensile behavior of a transparent polyurethane interlayer, *Materials & Design* 65 (2015) 1181-1188.
- [21] L. Zhang, X. Yao, S. Zang, Y. Gu, Temperature-and strain rate-dependent constitutive modeling of the large deformation behavior of a transparent polyurethane interlayer, *Polymer Engineering & Science*, 55 (2015) 1864-1872.
- [22] L. Zhang, X. Zhang, X. Yao, S. Zang, Experimental investigation on the tensile behavior of a transparent polyurethane interlayer, *International Journal of Materials Research*, 106 (2015) 996-1001.

- [23] Z. Liao, X. Yao, L. Zhang, M. Hossain, J. Wang, S. Zang, Temperature and strain rate dependent large tensile deformation and tensile failure behavior of transparent polyurethane at intermediate strain rates, *Int. J. Impact Eng*, 129 (2019) 152-167.
- [24] S. Wright, N. Fleck, W. Stronge, Ballistic impact of polycarbonate-an experimental investigation, *Int. J. Impact Eng*, 13 (1993) 1-20.
- [25] W. Toqueboeuf, B. Mortaigne, C. Cottenot, Dynamic behaviour of polycarbonate/polyurethane multi-layer for transparent armor, *Le Journal de Physique IV*, 7 (1997) C3-499-C493-504.
- [26] M. Timmel, S. Kolling, P. Osterrieder, P. Du Bois, A finite element model for impact simulation with laminated glass, *Int. J. Impact Eng*, 34 (2007) 1465-1478.
- [27] Y. Jialing, C. Xujie, W. Cunhao, Experimental and FEM study of windshield subjected to high speed bird impact, *Acta Mechanica Sinica*, 19 (2003) 543-550.
- [28] P.A. Hooper, R.A.M. Sukhram, B.R.K. Blackman, J.P. Dear, On the blast resistance of laminated glass, *Int J Solids Struct*, 49 (2012) 899-918.
- [29] S. Georgiadis, A.J. Gunnion, R.S. Thomson, B.K. Cartwright, Bird-strike simulation for certification of the Boeing 787 composite moveable trailing edge, *Composite Structures*, 86 (2008) 258-268.
- [30] M.A. Meyers, *Dynamic behavior of materials*, John wiley & sons, 1994.
- [31] M. Larcher, G. Solomos, F. Casadei, N. Gebbeken, Experimental and numerical investigations of laminated glass subjected to blast loading, *Int. J. Impact Eng*, 39 (2012) 42-50.
- [32] A. Mulliken, M. Boyce, Mechanics of the rate-dependent elastic-plastic deformation of glassy polymers from low to high strain rates, *Int J Solids Struct*, 43 (2006) 1331-1356.
- [33] J. Richeton, S. Ahzi, K. Vecchio, F. Jiang, R. Adharapurapu, Influence of temperature and strain rate on the mechanical behavior of three amorphous polymers: Characterization and modeling of the compressive yield stress, *Int J Solids Struct*, 43 (2006) 2318-2335.
- [34] D. Rittel, On the conversion of plastic work to heat during high strain rate deformation of glassy polymers, *Mechanics of Materials*, 31 (1999) 131-139.
- [35] P. Yu, X. Yao, Q. Han, S. Zang, Y. Gu, A visco-elastoplastic constitutive model for large deformation response of polycarbonate over a wide range of strain rates and temperatures, *Polymer*, 55 (2014) 6577-6593.
- [36] F. Rietsch, B. Bouette, The compression yield behaviour of polycarbonate over a wide range of strain rates and temperatures, *European Polymer Journal*, 26 (1990) 1071-1075.

- [37] S. Sarva, M. Boyce, Mechanics of polycarbonate during high-rate tension, *Journal of Mechanics of Materials and Structures*, 2 (2007) 1853-1880.
- [38] K. Cao, Y. Wang, Y. Wang, Effects of strain rate and temperature on the tension behavior of polycarbonate, *Materials & Design*, 38 (2012) 53-58.
- [39] K. Cao, X. Ma, B. Zhang, Y. Wang, Y. Wang, Tensile behavior of polycarbonate over a wide range of strain rates, *Materials Science and Engineering: A*, 527 (2010) 4056-4061.
- [40] M. Foster, B. Love, R. Kaste, P. Moy, The rate dependent tensile response of polycarbonate and poly-methylmethacrylate, *Journal of Dynamic Behavior of Materials*, 1 (2015) 162-175.
- [41] S. Tzibula, Z. Lovinger, D. Rittel, Dynamic tension of ductile polymers: Experimentation and modelling, *Mechanics of Materials*, 123 (2018) 30-42.
- [42] G. Mirone, The dynamic effect of necking in Hopkinson bar tension tests, *Mechanics of Materials*, 58 (2013) 84-96.
- [43] G. Mirone, D. Corallo, R. Barbagallo, Experimental issues in tensile Hopkinson bar testing and a model of dynamic hardening, *Int. J. Impact Eng*, 103 (2017) 180-194.
- [44] G. Mirone, R. Barbagallo, How sensitivity of metals to strain, strain rate and temperature affects necking onset and hardening in dynamic tests, *International Journal of Mechanical Sciences*, 195 (2021) 106249.
- [45] L. Zhang, G. Gour, N. Petrinic, A. Pellegrino, Rate dependent behaviour and dynamic strain localisation of three novel impact resilient titanium alloys: Experiments and modelling, *Mater. Sci. Eng. A*, 771 (2020) 138552.
- [46] L. Zhang, A. Pellegrino, D. Townsend, N. Petrinic, Strain rate and temperature dependent strain localization of a near α titanium alloy, *Int. J. Impact Eng*, 145 (2020) 103676.
- [47] R. Gerlach, C. Kettenbeil, N. Petrinic, A new split Hopkinson tensile bar design, *Int. J. Impact Eng*, 50 (2012) 63-67.
- [48] G. Quino, Y. Chen, K.R. Ramakrishnan, F. Martínez-Hergueta, G. Zumpano, A. Pellegrino, N. Petrinic, Speckle patterns for DIC in challenging scenarios: rapid application and impact endurance, *Measurement Science and Technology*, 32 (2020) 015203.
- [49] T. Chu, W. Ranson, M.A. Sutton, Applications of digital-image-correlation techniques to experimental mechanics, *Exp Mech*, 25 (1985) 232-244.
- [50] X. Poulain, L.W. Kohlman, W. Binienda, G.D. Roberts, R.K. Goldberg, A.A. Benzerga, Determination of the intrinsic behavior of polymers using digital image correlation combined with video-monitored testing, *Int J Solids Struct*, 50 (2013) 1869-1878.

- [51] G.T. Gray, III, Classic Split-Hopkinson Pressure Bar Testing, in: H. Kuhn, D. Medlin (Eds.) *Mechanical Testing and Evaluation*, ASM International, 2000, pp. 0.
- [52] F. De Cola, A. Pellegrino, C. Glößner, D. Penumadu, N. Petrinic, Effect of Particle Morphology, Compaction, and Confinement on the High Strain Rate Behavior of Sand, *Exp Mech*, 58 (2018) 223-242.
- [53] R. Othman, P. Guégan, G. Challita, F. Pasco, D. LeBreton, A modified servo-hydraulic machine for testing at intermediate strain rates, *Int. J. Impact Eng*, 36 (2009) 460-467.
- [54] S. Diot, D. Guines, A. Gavrus, E. Ragneau, Two-step procedure for identification of metal behavior from dynamic compression tests, *Int. J. Impact Eng*, 34 (2007) 1163-1184.
- [55] M. LeBlanc, D. Lassila, A hybrid technique for compression testing at intermediate strain rates, *Exp Techniques*, 20 (1996) 21-24.
- [56] O.S. Hopperstad, T. Børvik, M. Langseth, K. Labibes, C. Albertini, On the influence of stress triaxiality and strain rate on the behaviour of a structural steel. Part I. Experiments, *European Journal of Mechanics - A/Solids*, 22 (2003) 1-13.
- [57] S. Kweon, A.A. Benzerga, On the localization of plastic flow in glassy polymers, *European Journal of Mechanics - A/Solids*, 39 (2013) 251-267.
- [58] S. Sarva, A.D. Mulliken, M.C. Boyce, Mechanics of Taylor impact testing of polycarbonate, *Int J Solids Struct*, 44 (2007) 2381-2400.
- [59] J.A. Jansen, S. Technimet, Fractographic characterization of polycarbonate failure modes, in: *ANTEC-CONFERENCE PROCEEDINGS-, UNKNOWN*, 2004, pp. 4094-4099.
- [60] J. Lu, K. Ravi-Chandar, Inelastic deformation and localization in polycarbonate under tension, *Int J Solids Struct*, 36 (1999) 391-425.
- [61] J. Richeton, S. Ahzi, K. Vecchio, F. Jiang, A. Makradi, Modeling and validation of the large deformation inelastic response of amorphous polymers over a wide range of temperatures and strain rates, *Int J Solids Struct*, 44 (2007) 7938-7954.
- [62] G.R. Johnson, W.H. Cook, Fracture characteristics of three metals subjected to various strains, strain rates, temperatures and pressures, *Eng Fract Mech*, 21 (1985) 31-48.
- [63] A. Dwivedi, J. Bradley, D. Casem, Mechanical response of polycarbonate with strength model fits, in: *DYNAMIC SCIENCE INC ABERDEEN MD*, 2012.
- [64] G.R. Cowper, P.S. Symonds, Strain-hardening and strain-rate effects in the impact loading of cantilever beams, in: *Brown Univ. Tech. Rept. No. 28*, 1957.
- [65] D. Rittel, L.H. Zhang, S. Osovski, The dependence of the Taylor–Quinney coefficient on the dynamic loading mode, *J Mech Phys Solids*, 107 (2017) 96-114.

- [66] Z. Li, J. Lambros, Strain rate effects on the thermomechanical behavior of polymers, *Int J Solids Struct*, 38 (2001) 3549-3562.
- [67] Y. Tomita, S. Tanaka, Prediction of deformation behavior of glassy polymers based on molecular chain network model, *Int J Solids Struct*, 32 (1995) 3423-3434.
- [68] Y. Tomita, T. Adachi, P.S. Sik, Computational simulation of three-dimensional neck propagation in polymeric specimens under tension and hybrid identification of constitutive equation, *International Journal of Mechanical Sciences*, 39 (1997) 913-923.
- [69] V. Abaqus, 6.14 Documentation, Dassault Systemes Simulia Corporation, 651 (2014).
- [70] F. Dunne, N. Petrinic, *Introduction to Computational Plasticity*, 2005.
- [71] E. Parsons, M. Boyce, D. Parks, An experimental investigation of the large-strain tensile behavior of neat and rubber-toughened polycarbonate, *Polymer*, 45 (2004) 2665-2684.